Nuclear Engineering and Technology 51 (2019) 257–262

Contents lists available at ScienceDirect

Nuclear Engineering and Technology

journal homepage: www.elsevier.com/locate/net

Original Article

Influences of heating processes on properties and microstructure of porous CeO_2 beads as a surrogate for nuclear fuels fabricated by a microfluidic sol-gel process

Tong Song, Lin Guo, Ming Chen, Zhen-Qi Chang*

School of Nuclear Science and Technology, University of Science and Technology of China, Huang-Shan Road, He-Fei, PR China

ARTICLE INFO

Article history:
Received 2 December 2017
Accepted 28 September 2018
Available online 28 September 2018

Keywords:
Nuclear fuel
Microfluidics
Porous CeO_2 microspheres
Heating processes
Microstructure

ABSTRACT

The control of microstructure is critical for the porous fuel particles used for infiltrating actinide nuclides. This study concerns the effect of heating processes on properties and microstructure of the fuel particles. The uniform gel precursor beads were synthesized by a microfluidic sol-gel process and then the porous CeO_2 microspheres, as a surrogate for the ceramic nuclear fuel particles, were obtained by heating treatment of the gel precursors. The fabricated CeO_2 microspheres have a narrow size distribution and good sphericity due to the feature of microfluidics. The effects of heating processes parameters, such as heating mode and peak temperatures on the properties of microspheres were studied in detail. An optimized heating mode and the peak temperature of 650°C were selected to produce porous CeO_2 microspheres. The optimized heating mode can avoid the appearance of broken or crack microspheres in the heating process, and as-prepared porous microspheres were of suitable pore size distribution and pore volume for loading minor actinide (MA) solution by an infiltration method that is used for fabrication of MA-bearing nuclear fuel beads. After the infiltration process, 1000°C was selected as the final temperature to improve the compressive strength of microspheres.

1. Introduction

Though represent at a very low content, the minor actinides (MA) as the long-lived radionuclides are responsible for the bulk of the radiotoxicity of spent nuclear fuels, and are of major environmental concern. Transmutation of MA by specific nuclear reactor such as fast reactor (FR) and accelerator driven systems (ADS) is the most promising option to reduce nuclear waster radiotoxicity. Currently, a heterogeneous way of a MA-bearing nuclear fuel bead diluted in an inert metallic (CERMET) or ceramic (CERCER) matrix is selected as ADS nuclear fuel for MA transmutation [1]. Due to the radiation hazard and high activity of MA, the fabrication of MA-bearing fuel beads should be a dust-free process. The infiltration method, namely that the porous PuO_2 beads as the adsorbent carrier were fabricated by sol-gel processes, and then a MA nitrate solution was infiltrated in the porous beads, is an effective approach to synthesize these materials. In particular the process steps are simpler and no liquid waste is produced.

Considering that a spherical bead has the lowest surface area, it is clear that spherical beads will lead to the least damage within the inert matrix for the dispersed nuclear fuel [2]. Thus, spherical nuclear particles with uniform size are ideal. A capillary-based microfluidic technique has recently been developed as an effective approach for the fabrication of uniform-size particles [3] and provides a way to synthesize spherical porous PuO_2 carrier with a narrow size distribution.

As a carrier for loading MA solution, the pore structure of porous PuO_2 beads plays an important role in determining the efficiency of MA infiltration. It is well known that the preparation of porous materials by using porogen is a common method. Although the pore volume increases with increasing the addition quantity of porogen in some degree, porogen cannot control the pore structure, especially the pore size distribution. However, the pore size distribution, as well as the pore volume, has a significant effect on the infiltration effect. On the one hand, the infiltration efficiency cannot be improved by increasing micropores greatly as the size of them were too small to allow the solutions to infiltrate into the pores [4]. On the other hand, the excessively large-size pores cause a reduction in capillary tension [5], which leads to an unstable status of the

* Corresponding author.
E-mail address: zqchang@ustc.edu.cn (Z.-Q. Chang).

https://doi.org/10.1016/j.net.2018.09.022

absorbed solution. To overcome the above issues, the control of the pore structure parameters, especially the pore size distribution, is therefore of particular importance. Actually, the pore characteristics of microspheres are largely affected by the heating processes due to the fact that the porous structure is performed by burning off the porogen from the beads during the heating process. As a result, it is of great significance to adjust the pore structure of microspheres for fitting infiltration by controlling the heating processes parameters. But very limited published works were related to the effects of heating processes on the properties of microspheres. Moreover, it is essential to select suitable heating mode to form oxide microspheres with good mechanical integrity to avoid emission of fine and highly contaminant particles during the handing step. Thus, it is reasonable for us to pay more attention to the heating processes.

In this work, the same gel precursor beads with uniform-size were synthesized by microfluidic technique and the influence of heating processes on properties and microstructure of the obtained porous microspheres was systematically studied. Cerium was used as a surrogate for plutonium in these studies due to physicochemical similarity between them [6]. The decomposition of gel precursor beads and crystallization of the obtained CeO_2 microspheres were characterized by thermogravimetry and differential thermal analysis (TG/DTA) and X-ray diffraction (XRD). The microstructure and pore characteristics of the CeO_2 microspheres were studied through the scanning electron microscopy (SEM) and the surface area and porosimetry analyzer. The mechanical property of single microsphere was also assessed.

2. Materials and methods

2.1. Capillary-based microfluidic device

The microfluidic device was composed of a hydrophilic capillary (fused silica tubing, Polymicro Technologies) with an inner diameter/outer diameter of 250μm/360μm, a PTFE tubing (polytetrafluroethylene, Fisher Scientific Bioblock) with an inner diameter/outer diameter of 1.6mm/3.2 mm, a T-junction (P-728-01, Upchurch Scientific), and two syringes and two syringe pumps (LSP01-1A, Longer Pump).

As shown in Fig. 1, a capillary was inserted into the T-junction along its main axis. The continuous and dispersed phases, delivered by means of the two syringe pumps, were infused into two separate inlets of the T-junction. At the capillary's tip in the center of the outlet PTFE tubing, the dispersed phase was broken up to release a free-flowing droplet under shear forces imposed by the flow of the continuous phase. Transported by the continuous flow in the PTFE tubing, the droplets were heated by a 90°C water bath downstream and collected in a vessel.

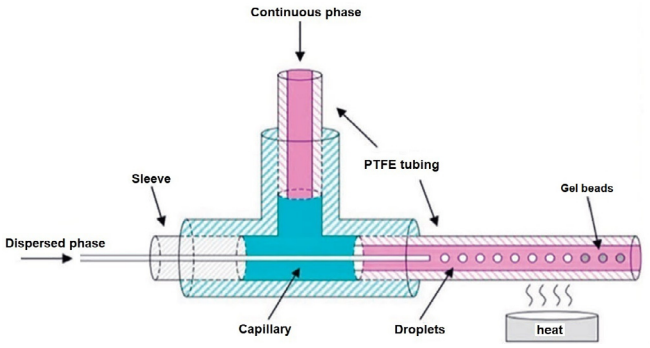

Fig. 1. Schematic of the capillary-based microfluidic device for the preparation of gel beads.

2.2. Materials

The following materials were used: for the dispersed phase, ammonium ceric nitrate $(NH_4)_2Ce(NO_3)_6$ (AR, Sinopharm Chemical Reagent Co., Ltd), urea $CO(NH_2)_2$ (AR, Shanghai Suyi Chemical Reagent Co., Ltd), hexamethylenetetramine (HMTA) $(CH_2)_6N_4$ (AR, Tianjin Guangfu Science and Technology Development Co., Ltd), polyethylene glycol 6000 (PEG 6000) (AR, Sinopharm Chemical Reagent Co., Ltd) and distilled water; for the continuous phase, dimethyl silicone oil (AR, Sinopharm Chemical Reagent Co., Ltd); for washing, ammonia solution (AR, Sinopharm Chemical Reagent Co., Ltd), petroleum ether 60°C to 90°C (AR, Sinopharm Chemical Reagent Co., Ltd); and for pore volume test, europium nitrate hexahydrate $Eu(NO_3)_3 \cdot 6H_2O$ (AR, Yangzhou Dingxin Technology Co., Ltd).

2.3. Fabrication of microspheres

The main fabrication process of microspheres is shown in Fig. 2, and its detailed process steps are as follows:

2.3.1. Synthesis of gel precursors

For the gel precursor beads production, ammonium ceric nitrate solution was mixed with urea and HMTA solutions under cool temperatures (0~5°C). To this feed solution, PEG 6000 (the mass ratio PEG 6000/$(NH_4)_2Ce(NO_3)_6$ was 30%) was added as porogen. The mixture was used as the dispersed phase and was injected into the microfluidic device. The monodisperse droplets were formed at the exit of the capillary upon contact with the continuous phase. After being heated by the 90°C water bath downstream, the droplets were transformed into gel beads. To complete the gelation process, the gel beads were collected and kept for 10 h in ammonia solution. Subsequently, the gel beads were washed with petroleum ether to remove the silicone oil and dried in air at room temperature for 5 h.

2.3.2. Heating processes

A muffle furnace (KSL-1700X, Hefei Kejing Materials Technology Co., Ltd) was used to heat the gel precursor beads in air atmosphere. The beads were placed as a single layer in a corundum crucible. Heating rates of 1°C/min, 2°C/min, 5°C/min, and 10°C/min were tested. Peak temperatures of 460°C, 600°C, 650°C, 700°C, 800°C,

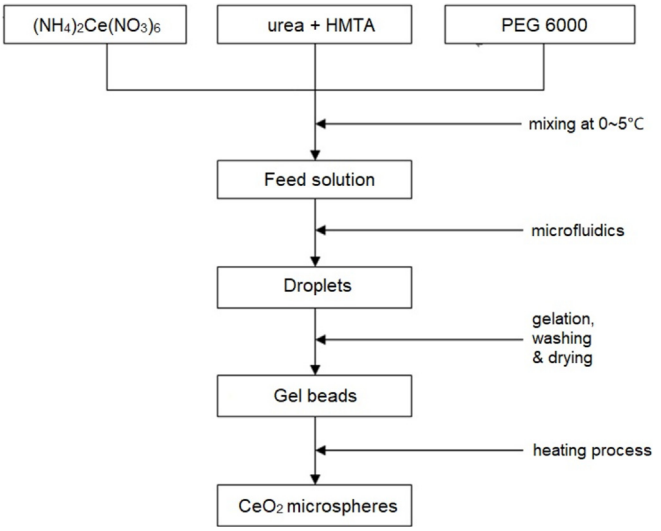

Fig. 2. Flow chart for fabricating the CeO_2 microspheres.

and 1000°C were tested. After the heating process, the muffle furnace was cooled down to room temperature by 3°C/min.

2.4. Characterization

The thermal behavior of the gel precursor beads was investigated by TG/DTA (DTG-60H, Shimadzu Co., Ltd). This was done in air at a constant heating rate of 10°C/min from room temperature to 1000°C.

The CeO_2 microspheres were observed by an optical microscope (XSP-30E, Shanghai Halibut Instrument Limited Company) equipped with a charge-coupled-device camera (uEye UI-2220SE, IDS) capturing up to 52 frames/s at full resolution (768 × 576 pixels). The diameters of microspheres were measured with an image analysis software (uEye Cockpit).

The crystallographic structure of CeO_2 microspheres was characterized by XRD (TTR-III, Rigaku Industrial Co., Ltd) using Cu Kα radiation at a scanning rate of 2°/min from 20° to 80°. The average crystallite size of CeO_2 microspheres was estimated from the full width at half maximum (FWHM) of the most intense diffraction line using the Scherrer's equation [7].

The microstructure analysis of CeO_2 microspheres was carried out by SEM (KYKY-AMRAY 1000B, Scientific Instrument Factory of Chinese Academy of Sciences). Both the surface and cross section SEM micrographs of CeO_2 microspheres were obtained.

The specific surface area, nitrogen adsorption-desorption isotherms, and pore size distribution of CeO_2 microspheres were measured by a surface area and porosimetry analyzer (V-sorb 2800, Gold APP Instruments Corporation).

The compressive strength of single microsphere was assessed by ZKD-microsphere (independently design and manufacture).

3. Results and discussion

3.1. Fabrication of size-controlled CeO_2 precursor beads

The reaction principles between urea, HMTA and heavy metal ions in the sol-gel process were introduced to synthesize CeO_2 gel precursors. Under cooled conditions (0–5°C), the complexes formed by the reaction between urea and cerium ions prevent hydrolysis of the metal ions. As temperature increases, the complexes and HMTA decompose. The decomposition of HMTA leads to a rise in pH of the sol, which induces gelation [8].

The size distribution of the gel precursors can be preciously controlled by controlling the sol droplets formation in the as-built microfluidic device as shown in Fig. 1. Our previous work had revealed that, the relationship between the droplet size, fluid flow rate, fluid viscosity and capillary size can be expressed with an empirical equation:

$$d_{drop}/d_{cap} = k(\mu_c \upsilon_c/\mu_d \upsilon_d)^{-0.22} \quad (1)$$

Where d_{drop} is the droplet diameter, d_{cap} is the internal capillary diameter, υ_c and υ_d are the dispersed and continuous flow rates, respectively, μ_c and μ_d are the viscosities of dispersed and continuous phases, respectively [9].

With a control of the fluids' flow rate, the uniform sol droplets and the consequent gel beads with a designated size as seen in Fig. 3(a) were formed, and size-controlled CeO_2 microspheres were obtained by calcining the gel beads, as presented in Fig. 3(b). The microspheres were of narrow size distribution with a coefficient of variation (CV) lower than 2.3%. The spherical shape of as-prepared microspheres was perfect and the average sphericity was below 1.05 which was defined as the ratio of its maximum diameter to minimum diameter [10]. The uniform nuclear fuel microspheres with a good sphericity provide a guarantee for the preparation of nuclide-homogeneous dispersion nuclear fuel.

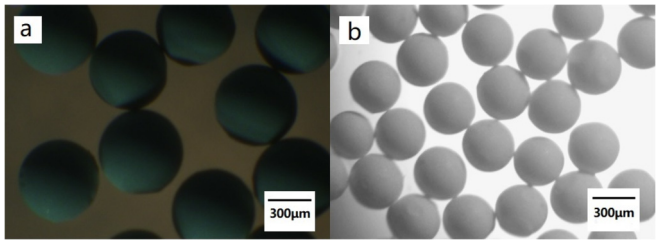

Fig. 3. Optical images of the microspheres: (a) the gel precursor beads produced by the microfluidic device; (b) the CeO_2 microspheres with diameter size of 364μm after the heating process. The flow rates for preparing the microspheres are 120μl/min (for the continuous phase) and 15μl/min (for the dispersed phase).

3.2. Heating processes and microstructure

Different heating processes were applied to the gel precursors to investigate the influence of the heating processes parameters on properties and microstructure of the porous CeO_2 microspheres.

3.2.1. Heating mode

The thermal behavior of the gel beads was analyzed by TG/DTA. Fig. 4 displays the TG/DTA profiles for gel beads. The first significant weight loss (12.5%) between room temperature and 137°C can be assigned to the loss of moisture, and the corresponding endothermic peak was at 72°C in the DTA curve. The exothermic effect noticed between 137 °C and 384°C can be ascribed to the elimination of organic gelification agents with a weight loss of 6.5%, which was accompanied by an exothermic peak at 204°C in the DTA curve. Above 384°C, crystallization of CeO_2 phase started and the weight loss was rather small (1.8%).

It is of great importance to keep microspheres intact for avoiding emission of small particles during the handing step. An excessive heating rate causes violent outgassing, leading to severe mechanical stress on the beads and their disintegration. Therefore, the principle of the temperature-rising strategy, on the one hand, is that the heating rate should be decreased; on the other hand, temperature should be held at the decomposition curve peak to allow the decomposition products to have enough time to escape to the surface of the green body completely. Based on the TG/DTA

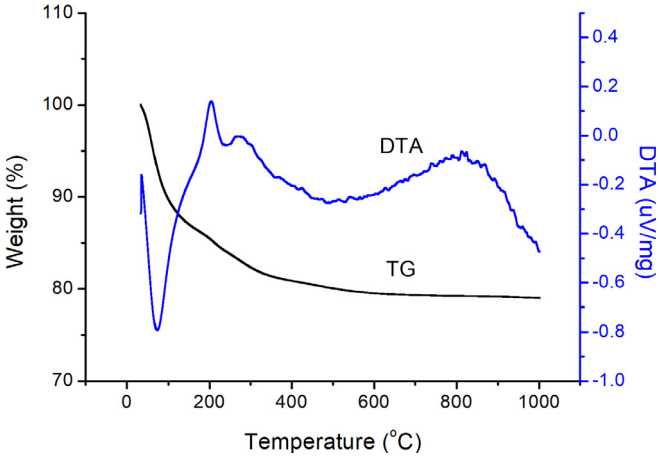

Fig. 4. TG/DTA thermograms of the gel beads.

analysis, 1 h dwelling time at 70°C and 200°C respectively was set during heating processes. Besides, 3 h dwelling time at peak temperature was set to complete the crystallization of CeO_2 phase. Then, the heating rates of 1°C/min, 2°C/min, 5°C/min, and 10°C/min were tested with a peak temperature of 800°C. The results show that the heating rate has an important influence on the microsphere fracture. The percentage of broken microspheres was declined from 12% at 10°C/min to 3% at 5°C/min. Moreover, there were neither broken nor crack microspheres found in samples obtained at 1°C/min or 2°C/min.

As shown in Fig. 5, the optimized heating mode based on the above discussion is set as follows: (1) 1 h dwelling time at 70°C and 200°C; (2) a slow heating rate of 2°C/min; and (3) 3 h dwelling time at peak temperature.

3.2.2. Peak temperature

Different peak temperatures (460°C, 600°C, 650°C, 700°C, 800°C and 1000°C) were tested to study the influence of peak temperatures on microspheres. The heating mode used in these tests was the optimized heating mode shown in Fig. 5.

Fig. 6 depicts the XRD patterns for products obtained by peak temperature of 460°C, 650°C, 800°C, and 1000°C. All the samples exhibited peaks consistent with the face-centered cubic (FCC) fluorite structure of CeO_2. The diffraction peaks became sharper with the increase of peak temperature, indicating the growth of the crystallite size of the samples. The corresponding mean crystallite size was 9, 16, 23, and 56 nm respectively.

The SEM images of the surface and cross section of the porous CeO_2 microspheres obtained at different peak temperatures are shown in Fig. 7. Compared with the slight increase of grain size between 460 °C and 650°C, the grain growth between 650°C and 1000°C was much larger. This means that sintering occurs at high peak temperatures.

The adsorption-desorption isotherms are shown in Fig. 8(a). All samples (except 460°C and 1000°C) exhibited the similar Type II adsorption-desorption isotherms, which is characteristic of macroporous materials. And the shape of the adsorption-desorption isotherms and the hysteresis loop were basically the same, but differing in quantity. Fig. 8(b) shows the corresponding pore size distributions of the samples. It can be seen that the pore size distributions strongly depend on the peak temperatures and the pore size increases with increasing peak temperature. Further observation from Fig. 8(b) indicates that the micropores declined sharply

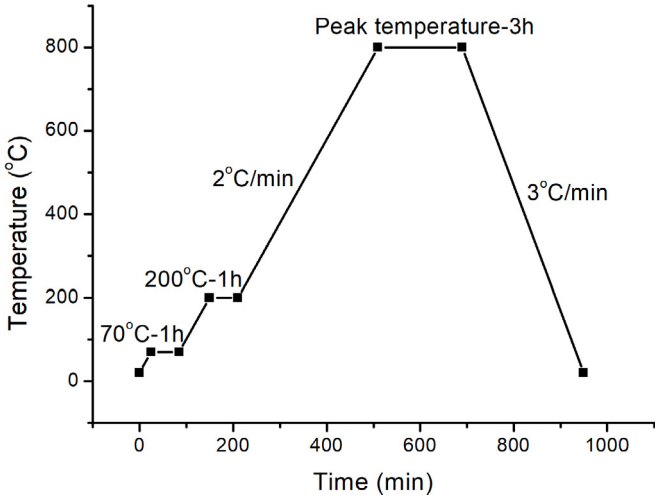

Fig. 5. The optimized heating mode.

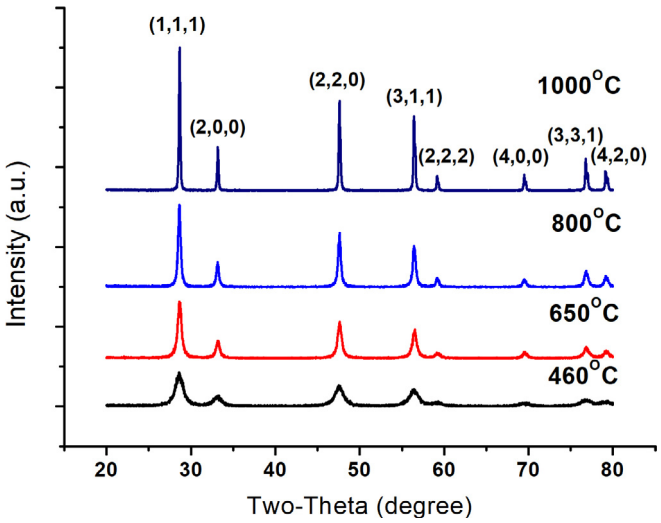

Fig. 6. XRD pattern of CeO_2 microspheres obtained at peak temperatures of 460°C, 650°C, 800°C, and 1000°C.

from 460°C to 650°C. This phenomenon is consistent with the dramatical decrease of specific surface area from 57.1 m^2/g at 460°C to 11.3 m^2/g at 650°C and can be attributed to the destruction of micropores and formation of macropores. Continue to increase peak temperature from 650°C, the crystal growing and aggregation [11] resulted in the diminishment of macropores below 200 nm. Relatively speaking, the pore size distribution of the microspheres obtained at 650°C is more suitable for infiltration compared with other peak temperatures.

The adsorption capacity of microspheres plays an important role in the efficiency of MA infiltration. The open pore volume that was available for infiltration was estimated by measuring the volume of

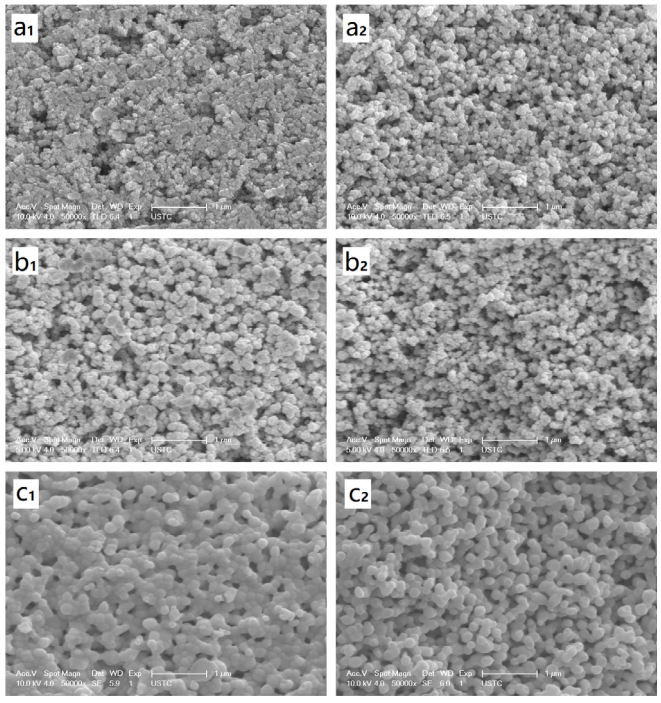

Fig. 7. SEM images for the surface (a_1, b_1, c_1) and cross section (a_2, b_2, c_2) of CeO_2 microspheres; scale bar is 1μm. The peak temperatures are (a_1, a_2) 460°C, (b_1, b_2) 650°C, and (c_1, c_2) 1000°C, respectively.

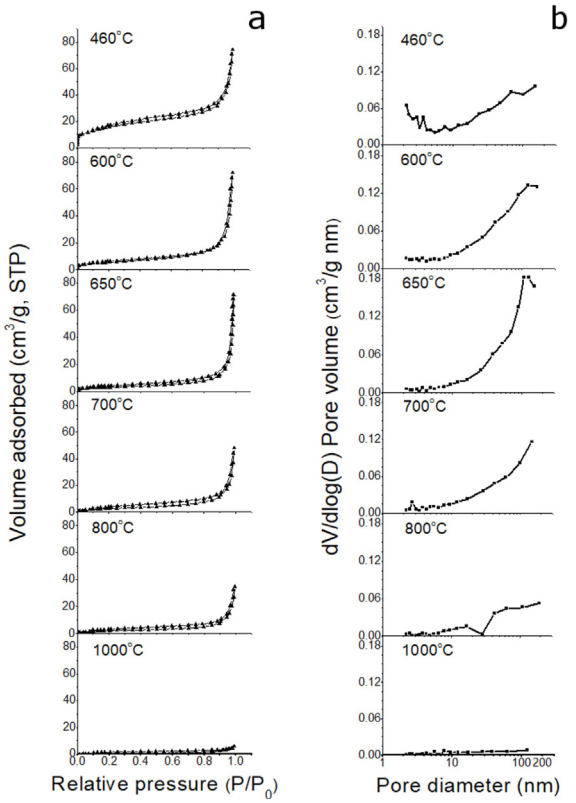

Fig. 8. The nitrogen adsorption-desorption isotherms (a) and the pore size distributions (b) of CeO_2 microspheres obtained at peak temperatures of 460°*C*, 600°*C*, 650°*C*, 700°*C*, 800°*C*, and 1000°*C*.

europium nitrate solution (as a surrogate for minor actinide nitrate solution [12]) infiltrated in the microspheres. This is meaningful as it provides tangible values to determine the maximum possible uptake of MA solution in microspheres. The infiltrated volume was defined as follows:

$$\theta = (1 - V_1/V_2) \times 100\% \quad (2)$$

Where θ is the infiltrated volume, V_1 is the increased volume of solution, V_2 is the volume of the sample, respectively. The volume of the sample was obtained from the number of microspheres and the volume of a single microsphere, which were determined from image analysis of a layer of microspheres with a narrow size distribution and perfect spherical shape [13]. These microspheres were completely immersed in the europium nitrate solution and infiltration process generated a large number of bubbles. When the bubbles were not generated, the increased volume of solution was measured.

As shown in Fig. 9, the infiltrated volume firstly increased about 22% from 460°*C* to 650°*C* because of the reduction of useless micropores and increase of useful macropores. Then, the infiltrated volume decreased about 32% from 650°*C* to 1000°*C* probably due to the densification of microsphere by the effect of sintering [14]. Therefore, the microspheres obtained at 650°*C* have more pore volume for infiltration than others. It can be found that pores obtained at peak temperature of 650°*C* are homogeneously distributed in the microsphere (Fig. 7(b_2)) and extend to the outer surface (Fig. 7(b_1)). These characteristics will beneficial for infiltrating minor actinide nitrate solution.

The higher compressive strength results in better mechanical stability of microspheres. Fig. 9 presents the results of the

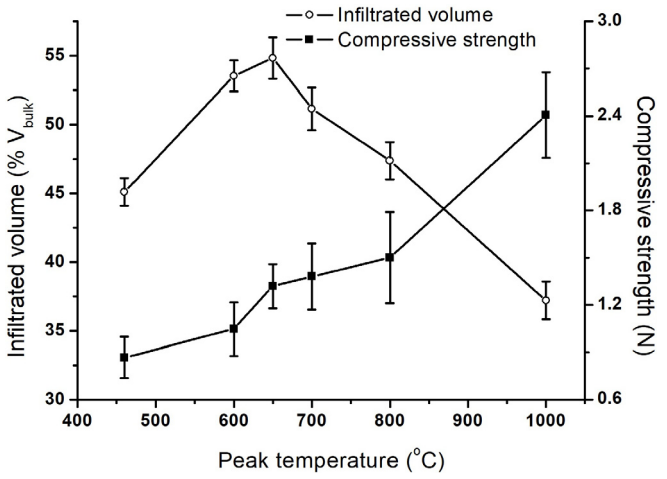

Fig. 9. Evolution of infiltrated volume and compressive strength of CeO_2 microspheres obtained at different peak temperatures.

compression test for the microspheres that were obtained at different peak temperatures. The average compressive strength increased with increasing the peak temperature. In particular, when the peak temperature was increased to 1000°*C*, the average compressive strength improved significantly. Considering that the MA-infiltrated microspheres are mixed with the powder matrix, followed by the compaction and sintering steps, higher compressive strength can reduce the damage of beads. In order to improve the compressive strength of microspheres, 1000°*C* was selected as the final temperature of the heating process after the infiltration process.

4. Conclusion

The porous CeO_2 microspheres with a narrow size distribution (CV < 2.3%) and good sphericity (d_{max}/d_{min} < 1.05), as a surrogate for the porous PuO_2 beads, were fabricated by calcining its precursors synthesized with a microfluidic sol-gel process.

Heating modes and peak temperatures for the calcination of the CeO_2 precursors have been investigated to optimize the mechanical properties and microstructure of the porous microspheres needed in loading minor actinides by an infiltration process. An hour dwelling time at 70°*C* and 200°*C* respectively and a slow heating rate of 2°C/min can avoid the appearance of broken or crack microspheres. CeO_2 microspheres calcined at a peak temperature of 650°*C* possessed more macropores and provided the maximum loading amount of europium nitrate solution as a surrogate of minor actinide nitrate solution. The average compressive strength of a porous microsphere obtained at 650°*C* was 1.3 N, which is strong enough to keep the microspheres from damage during infiltration operation. The results showed that the average compressive strength of the porous microsphere was strengthened by 82% as the peak temperature was increased from 650°*C* to 1000°*C*. In order to ensure high adsorption capacity and higher compressive strength of the microspheres, it suggested that the peak temperature of 650°*C* is applied to calcine CeO_2 precursors and then MA-infiltrated CeO_2 microspheres are sintered at final temperature of 1000°*C*.

Acknowledgements

Authors are grateful to National Nature Science Foundation of China for having funded this work through the grand No. 21076203 and No. 91226109. Authors thanks Chinese Academy of Sciences (No. XDA3010402) for financial support in the research.

References

[1] S. Pillon, J. Somers, S. Grandjean, J. Lacquement, Aspects of fabrication of curium-based fuels and targets, J. Nucl. Mater. 320 (2003) 36–43.

[2] N. Chauvin, R.J.M. Konings, H. Matzke, Optimisation of inert matrix fuel concepts for americium transmutation, J. Nucl. Mater. 274 (1999) 105–111.

[3] B. Ye, J.L. Miao, J.L. Li, Z.C. Zhao, Z.Q. Chang, C.A. Serra, Fabrication of size-controlled CeO_2 microparticles by a microfluidic sol-gel process as an analog preparation of ceramic nuclear fuel, J. Nucl. Sci. Technol. 50 (2013) 774–780.

[4] Z.F. Song, J. Wei, X. Li, W.Y. Zhou, Z.Q. Chang, C.A. Serra, Synthesis of size-controlled Pt/C/PTFE hydrophobic catalyst pellets in a capillary-based microfluidic system, Int. J. Hydrogen Energy 39 (2014) 16944–16952.

[5] R.J.M. Konings, D. Haas, Fuels and targets for transmutation, Compt. Rendus Phys. 3 (2002) 1013–1022.

[6] M. Osaka, S. Miwa, Y. Tachi, Simple fabrication process for CeO_2-MgO composite as surrogate for actinide-containing target for use in nuclear fuel, Ceram. Int. 32 (2006) 659–663.

[7] Z. Zhang, Y. Liu, G.C. Yao, Synthesis and characterization of dense and fine nickel ferrite ceramics through two-step sintering, Ceram. Int. 38 (2012) 3343–3350.

[8] V.N. Vaidya, Status of sol-gel process for nuclear fuels, J. Sol. Gel Sci. Technol. 46 (2008) 369–381.

[9] C. Serra, N. Berton, M. Bouquey, L. Prat, G. Hadziioannou, A predictive approach of the influence of the operating parameters on the size of polymer particles synthesized in a simplified microfluidic system, Langmuir 23 (2007) 7745–7750.

[10] K. Tsuchiya, H. Kawamura, Development of wet process with substitution reaction for the mass production of Li_2TiO_2 pebbles, J. Nucl. Mater. 283 (2000) 1380–1384.

[11] W.J. Zhang, C.G. Li, Z. Ma, L.L. Yang, H.B. He, Effects of calcination temperature on properties of 0.5%Al-3%In-TiO_2 photocatalyst prepared using sol-gel method, J. Adv. Oxid. Technol. 19 (2016) 119–124.

[12] M.V. Norton, F.A. DiGiano, R.T. Hallen, Selective separation of europium using polymer-enhanced ultrafiltration, Water Environ. Res. 69 (1997) 244–253.

[13] E. Remy, S. Picart, S. Grandjean, T. Delahaye, N. Herlet, P. Allegri, O. Dugne, R. Podor, N. Clavier, P. Blanchart, A. Ayral, Calcined resin microsphere pelletization (CRMP): a novel process for sintered metallic oxide pellets, J. Eur. Ceram. Soc. 32 (2012) 3199–3209.

[14] M. Mazaheri, A.M. Zahedi, M. Haghighatzadeh, S.K. Sadrnezhaad, Sintering of titania nanoceramic: densification and grain growth, Ceram. Int. 35 (2009) 685–691.